RARE METALS

ORIGINAL ARTICLE

Enhanced electromagnetic wave absorption properties of ZIF-67 modified polymer-derived SiCN ceramics by in situ construction of multiple heterointerfaces

Tao-Bo Geng, Gao-Yuan Yu, Gao-Feng Shao, Xiao-Gu Huang*

Abstract Multiphase polymer-derived ceramics have the advantages of thermal stability and adjustable dielectric properties, which exhibit significant potential for use in high-temperature microwave absorbing materials. Herein, Co-containing polymer-derived SiCN (Co–SiCN) ceramics were successfully synthesized by the physical mixing of zeolitic imidazolate framework (ZIF)-67 and polysilazane precursors and subsequent pyrolysis. The phase and chemical compositions, microstructures, dielectric properties, electromagnetic wave absorption (EWA) performance, and mechanism of the ceramics were investigated. The results showed that the introduction of ZIF-67 promoted the in situ formation of dielectric loss phases, including SiC nanocrystals, CoSi nanocrystals, and free carbon. The phase composition can be regulated by controlling the pyrolysis temperature to achieve ideal EWA properties. The Co–SiCN ceramic pyrolyzed at 1500 °C demonstrated excellent EWA performance, with a maximum effective absorption band (EAB_{max}) of 3.0 GHz at an ultralow thickness of 1.05 mm and minimum reflection loss (RL_{min}) of − 46.4 dB at a low frequency of 6 GHz. Compared with other reported SiCN-based ceramics containing magnetic metals, the ceramics prepared in this study stand out because of their low RL and high EAB at low thicknesses.

Tao-Bo Geng and Gao-Yuan Yu have contributed equally to this work.

T.-B. Geng, G.-Y. Yu, G.-F. Shao, X.-G. Huang*
School of Chemistry and Materials Science, Nanjing University of Information Science & Technology, Nanjing 210044, China
e-mail: hxg@nuist.edu.cn

The superior microwave absorption performance of the Co–SiCN ceramics is attributed to the heterointerface polarization, and impedance matching induced by the synergistic effects of their co-existing electromagnetic transparent/absorption phases. This study provides new insights into the development of high-performance SiCN-based microwave absorbers.

Keywords Polymer-derived SiCN ceramic; Multiple heterointerfaces; Zeolitic imidazolate framework (ZIF-67); Electromagnetic wave absorption (EWA)

1 Introduction

Rapid developments in stealth technology, such as radar and military equipment, and the popularization of electronic equipment and wireless communication technology have led to significant interest in high-performance microwave absorbers with strong absorption intensity, a broad effective absorption band, low thickness, and light weight [1–7]. The polymer-derived method presents a promising route for preparing high-performance ceramic-based microwave absorption materials owing to the unique advantages of polymer-derived ceramics, such as SiC [8], SiOC [9], SiCN [10], and SiBCN [11], in terms of thermal stability, corrosion, and oxidation resistance [8–10], as well as the tailorability of their precursor structure and convenient processing [11].

Among the reported polymer-derived ceramics (PDCs), SiCN ceramics stand out because of their lightweight, high thermal stability, and excellent dielectric properties. Therefore, they are applicable as dielectric loss materials in the field of microwave absorption [12, 13]. An increase in

the pyrolysis temperature promotes the formation of SiC nanocrystals, Si_3N_4 nanocrystals, and free carbon within the amorphous SiCN matrix, and SiC and free carbon can significantly enhance the electromagnetic wave loss capability of ceramics [14]. However, Li et al. [15] found that Si_3N_4 and SiC nanocrystals formed only when the annealing temperature exceeded 1500 °C. Such a high crystallization temperature severely hinders the application of PDCs as high-performance microwave absorbers. The crystallization temperature can be reduced by introducing transition metals such as Fe, Co, or Ni into the polymer, as these metals facilitate the crystallization behavior of the free carbon and SiCN components, and hence optimize the ceramic microstructure to tune the electromagnetic parameters and enhance electromagnetic wave attenuation [16–20].

Metal–organic frameworks (MOFs) are a class of crystalline porous materials composed of inorganic metal centers (metal ions or metal clusters) and bridged organic ligands that can be transformed into metal-doped carbon without significant structural changes when directly pyrolyzed [6, 21–23]. Luo et al. [11] prepared MOF/SiBCN absorbers by introducing ZIF-67 into a hyperbranched polyborosilazane matrix at a certain pyrolysis temperature to promote the in situ formation of dielectric loss phases, such as SiC nanocrystals, CoSi nanocrystals, and turbostratic carbons, within the amorphous ceramic matrix. The MOF/SiBCN ceramic exhibited excellent microwave absorption, with reflection loss values reaching − 51.6 dB at 9.36 GHz. This report revealed that MOFs could promote the crystallization behavior of SiBCN ceramics to induce the generation of high dielectric crystalline phases at a relatively low preparation temperature. However, to date, no reports on MOF-modified SiCN nanocomposites have been published. The development of such nanocomposites could guide the synthesis of high-performance SiCN-based microwave absorbers. The combination of these high dielectric crystalline phases with a SiCN ceramic matrix can promote the absorption of electromagnetic waves into the material interior, thereby optimizing impedance matching and enhancing the microwave absorption properties of the resulting composites.

In this study, we introduced zeolitic imidazolate framework (ZIF-67) into polysilazane preceramic precursors through a facile heat treatment process immediately after freeze-drying to fabricate Co-containing polysilazane-derived SiCN (Co–SiCN) ceramics with multiple heterointerfaces. The phase composition, microstructure, and dielectric and electromagnetic wave absorption (EWA) properties of the resultant Co–SiCN ceramics pyrolyzed at different temperatures were investigated. The results showed that the introduction of ZIF-67 facilitated the generation of nanocrystals and turbostratic carbons in the

SiCN ceramic matrix, which was beneficial to the microwave absorption properties of the ceramics. When the pyrolysis temperature reached 1500 °C, the ceramics demonstrated high EWA performance with a minimum reflection loss (RL_{min}) of − 46.4 dB at 2.7 mm and maximum effective absorption band (EAB_{max}) of 3.0 GHz at 1.05 mm. Compared with other reported SiCN-based ceramics containing magnetic metals, the Co–SiCN ceramics prepared in this study stand out because of their low RL and high EAB at a low thicknesses. The simple and efficient preparation method proposed herein provides a new approach for the development of high-performance SiCN-based microwave absorbers.

2 Experimental

2.1 Materials

Cobalt nitrate hexahydrate ($CO(NO_3)_2 \cdot 6H_2O$, 99.99 wt%), 2-methylimidazole (99 wt%), tert-butanol, and methyl alcohol were purchased from Shanghai Macklin Biochemical Co. Ltd. (China). The polymer precursor (polysilazane resin) was purchased from Kuberd Chemical Co. Ltd. (Shanghai, China). All chemicals were used as received, without additional purification.

2.2 Synthesis of ZIF-67

ZIF-67 was synthesized according to a previously reported method [24]. First, 0.98 g of cobalt nitrate hexahydrate and 4.42 g of 2-methylimidazole were separately dissolved in 50 ml of methyl alcohol by stirring. The two solutions were thereafter mixed and stirred for 1 h. After being stored at room temperature for 24 h, the mixture was transferred to a high-speed centrifuge, and the particles formed were collected via centrifugation at 8000 r·min^{-1}. Finally, the particles were washed three times with methanol and vacuum-dried at 60 °C. As shown in Fig. S1a and b, the as-synthesized ZIF-67 crystals present a rhombic dodecahedral structure with a size of approximately 50–100 nm.

2.3 Synthesis of Co–SiCN ceramics

Exactly 70 mg ZIF-67 was dissolved in 5 ml of tert-butanol, and the solution was ultrasonicated for 30 min. Subsequently, 7 g of polysilazane resin was dissolved in 5 ml of tert-butanol and rapidly stirred for 30 min. The two solutions were mixed by vigorous stirring and freeze-dried for 12 h. The obtained precursors were crosslinked at 300 °C for 2 h under an argon atmosphere (heating rate: 2 K·min^{-1}). The crosslinked precursors were ground into powders and pyrolyzed under an Ar atmosphere at 1300,

1400, or 1500 °C (heating rate: 2 K·min^{-1}, holding time: 3 h). For convenience, the samples were designated as S-1300, S-1400, and S-1500, according to their pyrolysis temperatures.
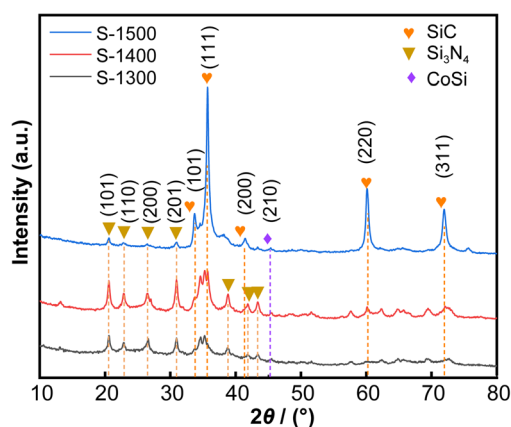
2.4 Characterization

X-ray diffraction (XRD) patterns were acquired using a Rigaku D/teX Ultra 250 detector with Cu Kα radiation (0.154 nm) at a generator voltage of 40 kV. X-ray photoelectron spectroscopy (XPS) measurements were performed on an ESCALAB250Xi (Thermo Fisher) using a monochromic Al Kα (photon energy (*hn*) = ¼1486.6 eV) X-ray source. Transmission electron microscopy (TEM) was performed at 200 kV using a Talos F200X instrument (Thermo Fisher Scientific). The dielectric constants of the ceramic powders were measured using a vector network analyzer (VNA, PNAN5244A, Agilent). The ceramic powders and paraffin wax were uniformly mixed at a mass ratio of 3:1, and the coaxial ring specimens were pressed with an outer diameter of 7.00 mm, an inner diameter of 3.00 mm.

3 Results and discussion

3.1 Phase composition and microstructures

Figure 1 shows the XRD patterns of the Co–SiCN ceramics. Si_3N_4 diffraction peaks and a weak CoSi diffraction peak centered at 45.1° appeared when the ceramic was pyrolyzed at 1300 °C. When the pyrolysis temperature was 1400 °C, the intensity of the Si_3N_4 peaks increased, thus suggesting that the increase in pyrolysis temperature improved the crystallinity of the composite. When the pyrolysis temperature was 1500 °C, three strong SiC peaks

appeared at 35.7°, 60°, and 71.8°, and the Si_3N_4 peaks became weak. This is because a higher pyrolysis temperature promotes the carbothermal reaction between free carbon and Si_3N_4, as expressed in Eq. (1):

$$Si_3N_4(s) + 3C(s) \rightarrow 3SiC(s) + 2N_2(g) \qquad (1)$$
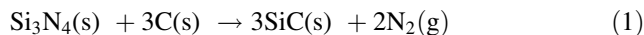
The XRD patterns revealed that the pyrolysis temperature played an important role in the final phase composition of the Co–SiCN ceramics.

The phase composition and microstructure of S-1500 were further investigated using TEM. SiC and Si_3N_4 nanocrystals as well as amorphous SiCN were observed in the HRTEM images. As shown in Fig. 2a–c, crystalline SiC and Si_3N_4 phases were observed in the amorphous SiCN matrix. The selected area electron diffraction (SAED) pattern in Fig. 2d shows two polycrystalline diffraction rings, which can be assigned to the SiC (111) and Si_3N_4 (320) planes. The TEM results were consistent with the XRD patterns. ZIF-67 induces the in situ generation of SiC, Si_3N_4, and CoSi, which provides a large number of heterogeneous interfaces. The large number of grain boundaries between the amorphous and crystalline phases (Si_3N_4, SiC, and CoSi) or different crystalline phases promote the interfacial polarization of the SiCN ceramics, ultimately improving their EWA performance.

3.2 Chemical composition

XPS profiles of the Co–SiCN ceramics shown in Fig. 3 reveal O 1s, N 1s, C 1s, Si 2s, and Si 2p peaks. For all three samples, the C 1s peaks were deconvoluted into four peaks: C–Si (283.5 eV), C=C (284.6 eV), C–C (285.8 eV), and C–O (289.1 eV) [25]. The Si 2p spectrum could be separated into three peaks at 101.5, 102.3, and 103.2 eV, which are assigned to the Si–C, Si–N, and Si–O bonds, respectively. As the pyrolysis temperature increased from 1300 to 1500 °C, the relative content of C–C slightly decreased, whereas the content of C–Si bonds significantly increased. These change trends are attributed to the increase in the graphitization degree of free carbon with increasing pyrolysis temperature and the extensive situ generation of SiC when the ceramics were pyrolyzed at 1500 °C, respectively. A comparison of the Si 2p spectra of S-1300, S-1400, and S-1500 revealed that the relative contents of Si–O and Si–N bonds significantly decreased, whereas the relative contents of Si–C bonds gradually increased with increasing pyrolysis temperature. Therefore, increasing the pyrolysis temperature appears to promote reactions between the free carbon and the O- or N-containing phases within the SiCN ceramics, thereby reducing the relative contents of O and N and encouraging the growth of the SiC phase.

Fig. 1 XRD patterns of Co–SiCN ceramics pyrolyzed at different temperatures
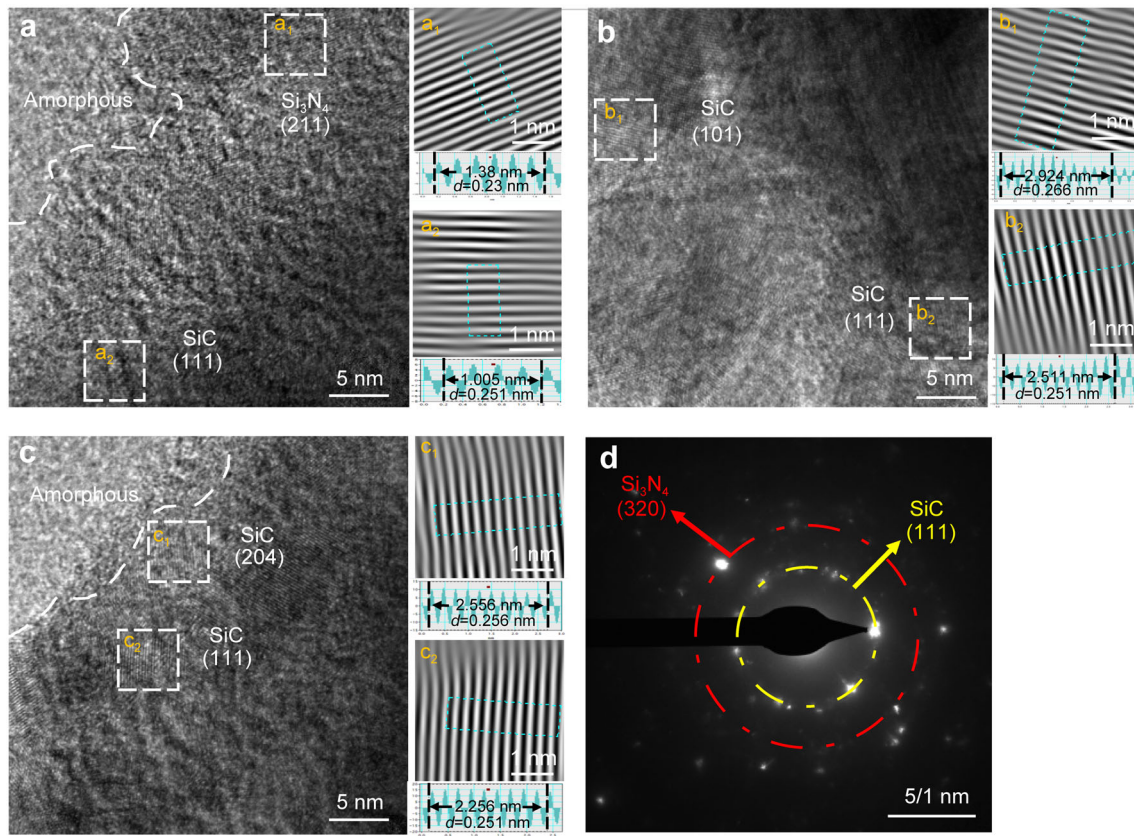
Fig. 2 **a**−**c** HRTEM images and corresponding inverse fast Fourier transform (IFFT) images; **d** SAED pattern of sample S-1500
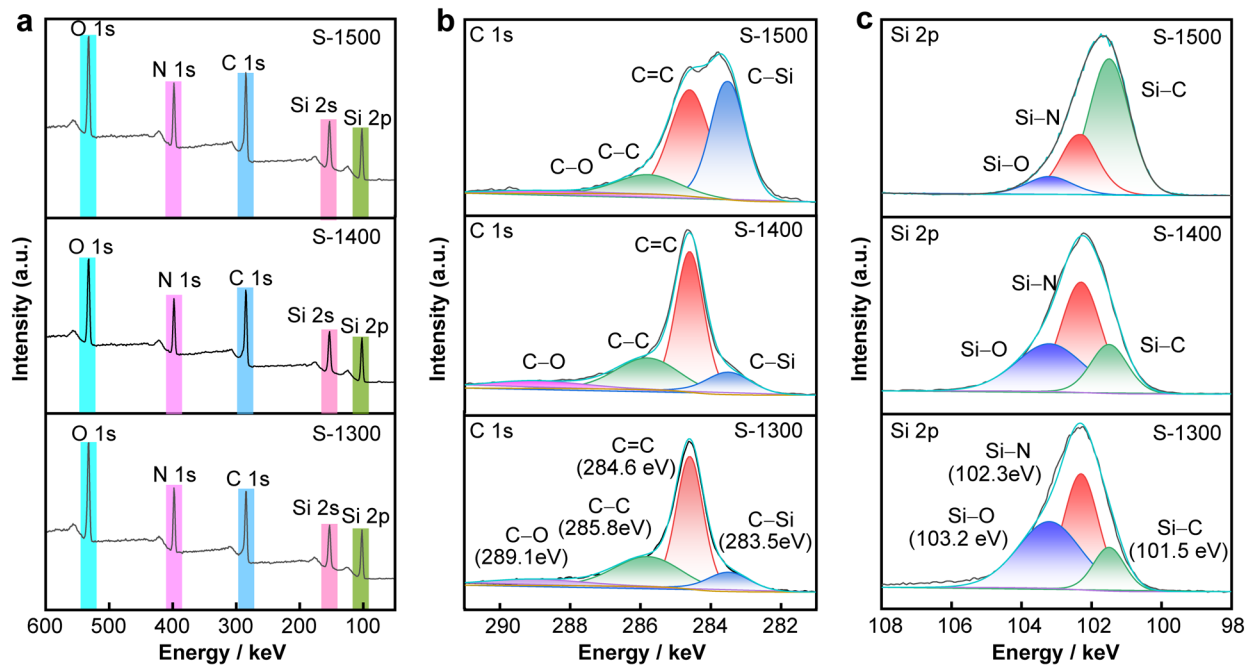
Fig. 3 XPS spectra of Co–SiCN ceramics pyrolyzed at different temperatures: **a** survey, **b** C 1s, **c** Si 2p

3.3 EWA performance

RL, EAB, and thickness are the main indices used to evaluate the EWA performance of ceramics pyrolyzed at various temperatures [26, 27]. According to the transmission line theory, RL can be calculated from the measured complex electromagnetic parameters, as described in the following formulas [28–30]:

$$RL = 20 \lg \left| \frac{Z_{in} - Z_0}{Z_{in} + Z_0} \right| \qquad (2)$$

$$Z_{in} = Z_0 \sqrt{\frac{\mu_r}{\varepsilon_r}} \tanh \left(j \frac{2\pi f d \sqrt{\mu_r \varepsilon_r}}{c} \right) \qquad (3)$$

where Z_{in} denotes the input characteristic impedance, Z_0 denotes the impedance of air, μ_r denotes relative complex permeability, ε_r denotes the relative complex permittivity, c denotes the velocity of light, f denotes the frequency of the waves, and d denotes the thickness of the ceramic. An RL value below $- 10$ dB corresponds to an absorption of 90% of the incident electromagnetic waves, and the corresponding frequency range is defined as the EAB.

Figure 4a–c shows the three-dimensional (3D) RL maps of S-1300, S-1400 and S-1500, which clearly reflect the increasing EWA properties of the ceramic samples with increasing pyrolysis temperature. In contrast to S-1300 and S-1400 which exhibit peak RL_{min} values at a high frequency, S-1500 exhibits an RL_{min} at a low frequency, as well as enhanced EWA properties at a high frequency.

The corresponding RL curves of the Co–SiCN ceramics pyrolyzed at different temperatures are shown in Fig. 4d–f. RL_{min} and EAB_{max} of S-1300 were $- 15$ dB and 1.6 GHz at 5 mm, respectively (Fig. 4d). RL_{min} and EAB_{max} of S-1400 reach $- 18.9$ dB at 1.1 mm and 2.6 GHz at 1.3 mm, respectively (Fig. 4e). When the pyrolysis temperature increased to 1500 °C, the resultant ceramic achieved excellent EWA performance, as evidenced by its EAB_{max} of 3.0 GHz at an ultralow thickness of 1.05 mm and RL_{min} of $- 46.4$ dB at a low frequency of 6 GHz.

In general, high-performance SiCN-based microwave absorbers require strong absorption and a broad bandwidth at low thicknesses. The RL and EAB values of S-1300, S-1400, and S-1500 at thicknesses of 1, 1.05, 1.1, 1.2, and 1.3 mm are compared in Fig. 5a, b. As the pyrolysis temperature increased, the RL and EAB values obtained at lower thicknesses approached the ideal values. Interestingly, the Co–SiCN ceramics pyrolyzed at 1500 °C can simultaneously achieve a low RL value of $- 40.5$ dB and a high EAB value of 3 GHz at an ultralow thickness of 1.05 mm. These findings can inspire the design and synthesis of thin electromagnetic wave absorbing materials.

The EWA performances of the prepared ceramics were compared with those of previously reported SiCN-based ceramics containing magnetic metals (summarized in
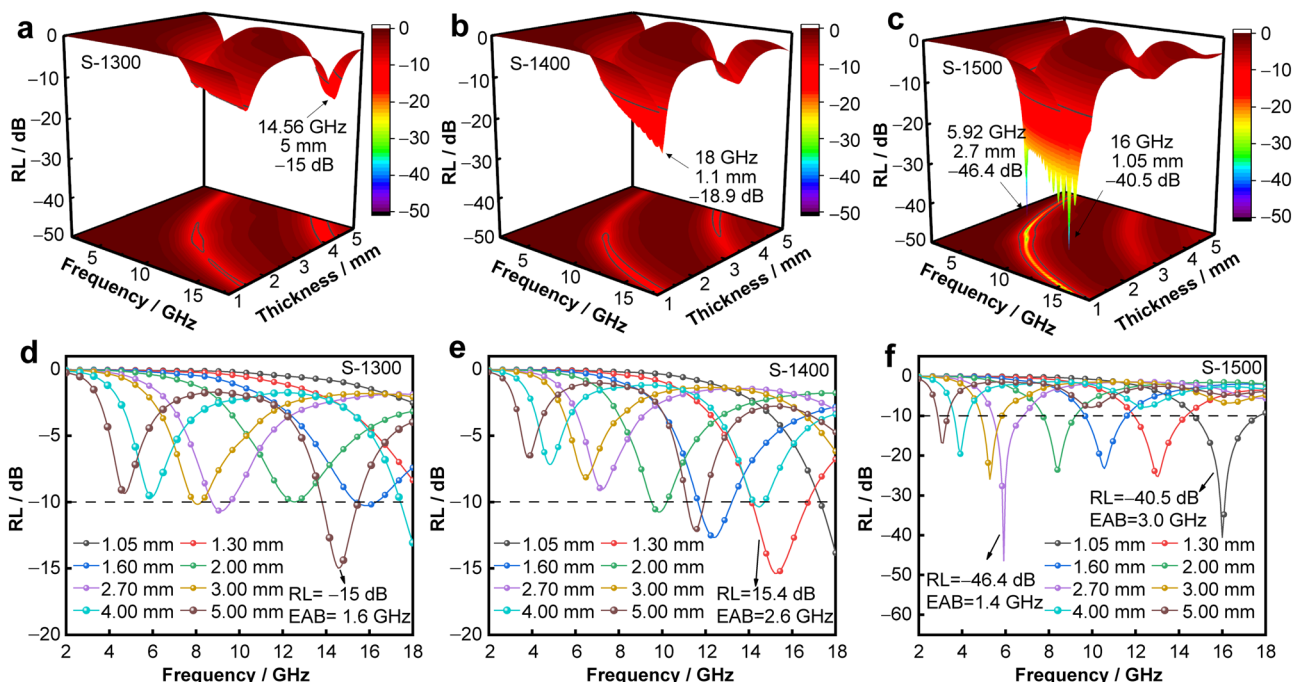
Fig. 4 3D plots of RL and RL curves of Co–SiCN ceramics pyrolyzed at different temperatures: **a**, **d** S-1300, **b**, **e** S-1400 and **c**, **f** S-1500
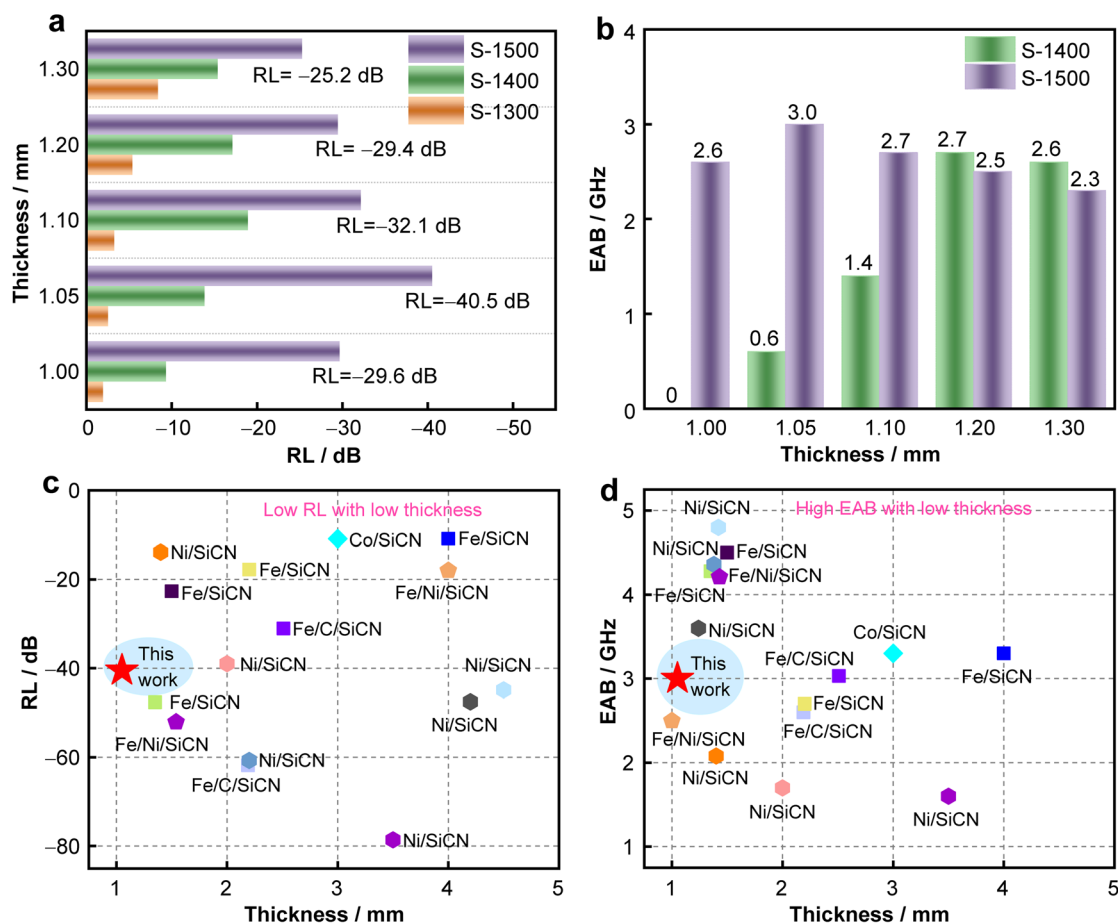
Fig. 5 a Comparison of RL values and **b** EAB values with corresponding thickness of Co–SiCN ceramics pyrolyzed at different temperatures; **c**, **d** comprehensive comparison of EWA performance considering RL_{min}, EAB_{max} and thickness with reported SiCN-based ceramic containing magnetic metal, which are listed in Table S1 in Supporting Information

Table S1) in terms of RL_{min}, EAB_{max}, and thickness, as shown in Fig. 5c, d. The SiCN ceramics prepared in this study stand out among the reported magnetic metal containing SiCN-based ceramic EWA materials because of their low RL and high EAB at low thicknesses.

3.4 Dielectric properties

SiCN ceramics are dielectric loss materials with electromagnetic absorption behaviors that can be attributed to the synergistic effects of polarization loss and conductivity loss [31, 32]. The dielectric properties of S-1300, S-1400, and S-1500 are shown in Fig. 6a–c. According to Debye theory, the real permittivity (ε') which is dependent on the electric energy stocking capacity represents the polarization capability of a material, whereas the imaginary permittivity (ε'') which is related to the polarization relaxation produced by dipole polarization and conductivity loss represents its ability to dissipate electromagnetic energy [33–35].

As shown in Fig. 6a, b, the ε' and ε'' values exhibit an approximately increasing trend with increasing pyrolysis temperature. This trend could be attributed to the effect of abundant polarization mechanisms, including interfacial polarization between multiple heterointerfaces, dipole polarization of SiC, free carbon, and defect polarization due to defects and dangling bonds in free carbons. S-1500 also exhibits the highest tanδ value (2–18 GHz), which indicates that it has the best dielectric loss capability among the samples.

The Cole–Cole semicircles of S-1300, S-1400, and S-1500 are shown in Fig. 6d–f to clarify the dissipation mechanisms of their dielectric polarization. According to the Debye theory, the relationship between ε' and ε'' can be described as follows [36–38]:

$$\left(\varepsilon' - \frac{\varepsilon_{(s)} + \varepsilon_{\infty}}{2}\right)^2 + (\varepsilon'')^2 = \left(\frac{\varepsilon_{(s)} - \varepsilon_{\infty}}{2}\right)^2 \quad (4)$$

where ε_s represents the static permittivity and ε_{∞} means the relative dielectric permittivity at limiting high frequency.
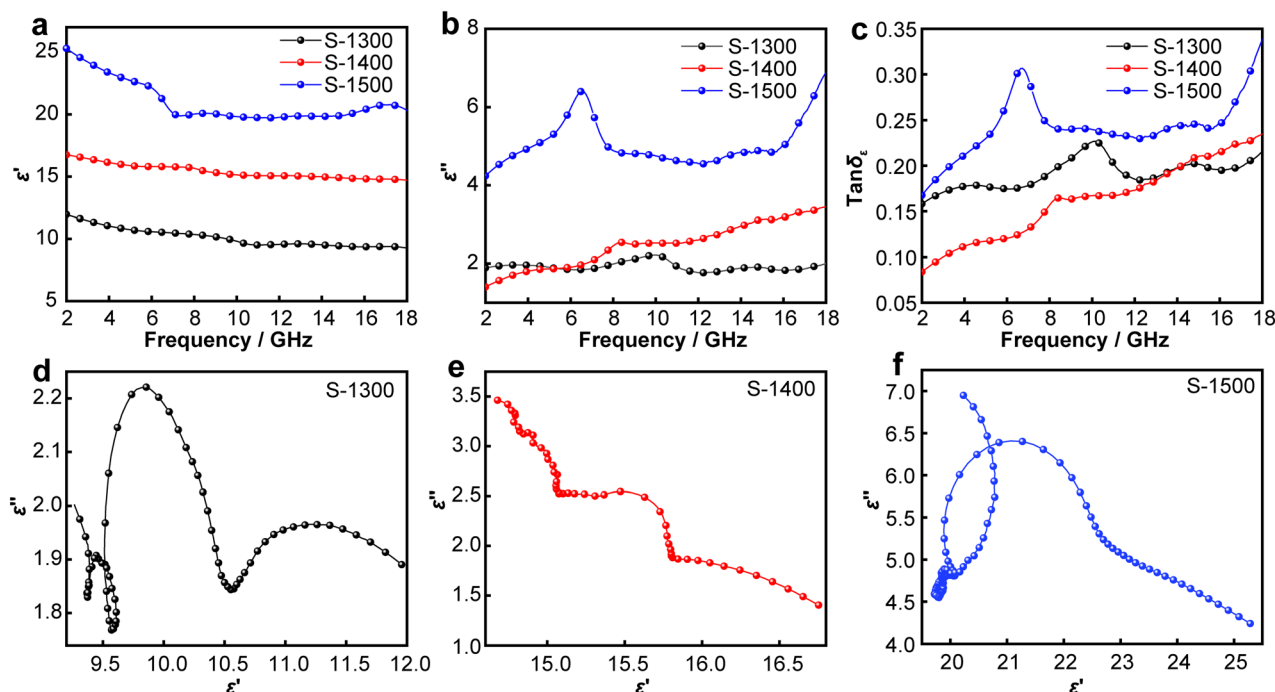
Fig. 6 a Real and **b** imaginary parts of complex permittivity; **c** dielectric loss tangent; **d–f** Cole–Cole curves of Co–SiCN ceramics pyrolyzed at different temperatures

In general, the Cole–Cole semicircle intuitively represents the dielectric polarization of a microwave absorbing material. As shown in Fig. 6d–f, all three samples present clear semicircles, which suggests that polarization is the most important dielectric loss mechanism of the Co–SiCN ceramics. Among the samples, S-1500 exhibits the strongest dielectric polarization which includes the interface polarization between SiC nanocrystals, Si_3N_4 crystals, and amorphous SiCN, and the dipole polarization of SiC nanocrystals and free carbon.

The impedance matching value (Z_{in}) and attenuation coefficient (α) which are two important parameters that determine the RL value of a material, were calculated as follows [39–42]:

$$\alpha = \frac{\sqrt{2}\pi f}{c} \times \sqrt{(\mu''\varepsilon'' - \mu'\varepsilon') + \sqrt{(\mu''\varepsilon'' - \mu'\varepsilon')^2 + (\mu''\varepsilon' - \mu'\varepsilon'')^2}} \tag{5}$$

After analyzing the dielectric loss properties of the Co–SiCN ceramics, two-dimensional (2D) impedance matching images of S-1300, S-1400, and S-1500 were plotted to investigate why Co–SiCN ceramics pyrolyzed at different temperatures exhibit different microwave absorption properties. As shown in Fig. 7a–c, S-1300 and S-1400 have poorer impedance matching characteristics compared with S-1500, the impedance matching value of

which is much greater than 1.0, owing to their lack of high dielectric loss phases. S-1500 demonstrates optimal Z_{in} values at both low- and high-frequency ranges, which may be attributed to the generation of crystalline phases, such as the SiC phase, which introduces more interfaces into the SiCN matrix.

RL_{min} and EAB_{max} of S-1500 can reach -40.5 dB and 3.0 GHz, respectively. The Z_{in} and α values of S-1300, S-1400, and S-1500 shown in Fig. 7d and e indicate that S-1500 has the best impedance matching characteristics and the largest attenuation coefficient, leading to its excellent EWA ability. A comparison of the Z_{in}, α, and RL curves of S-1500 at 1.05 mm is plotted in Fig. 7f to determine the origin of its maximum absorption peak. The maximum absorption peak is located exactly at the frequency where Z_{in} is equal to 1.0, and α is relatively high at 2–18 GHz.

3.5 EWA mechanism

The aforementioned results reveal that the Co–SiCN ceramic pyrolyzed at 1500 °C exhibits the optimal EWA properties among the samples. The absorption mechanism of S-1500 is illustrated in Fig. 8. The composition of S-1500 comprised an amorphous SiCN matrix, crystalline Si_3N_4, SiC, CoSi, and free carbon, forming a typical microstructure coexisting with electromagnetic transparent and absorption phases. The electromagnetic transparent
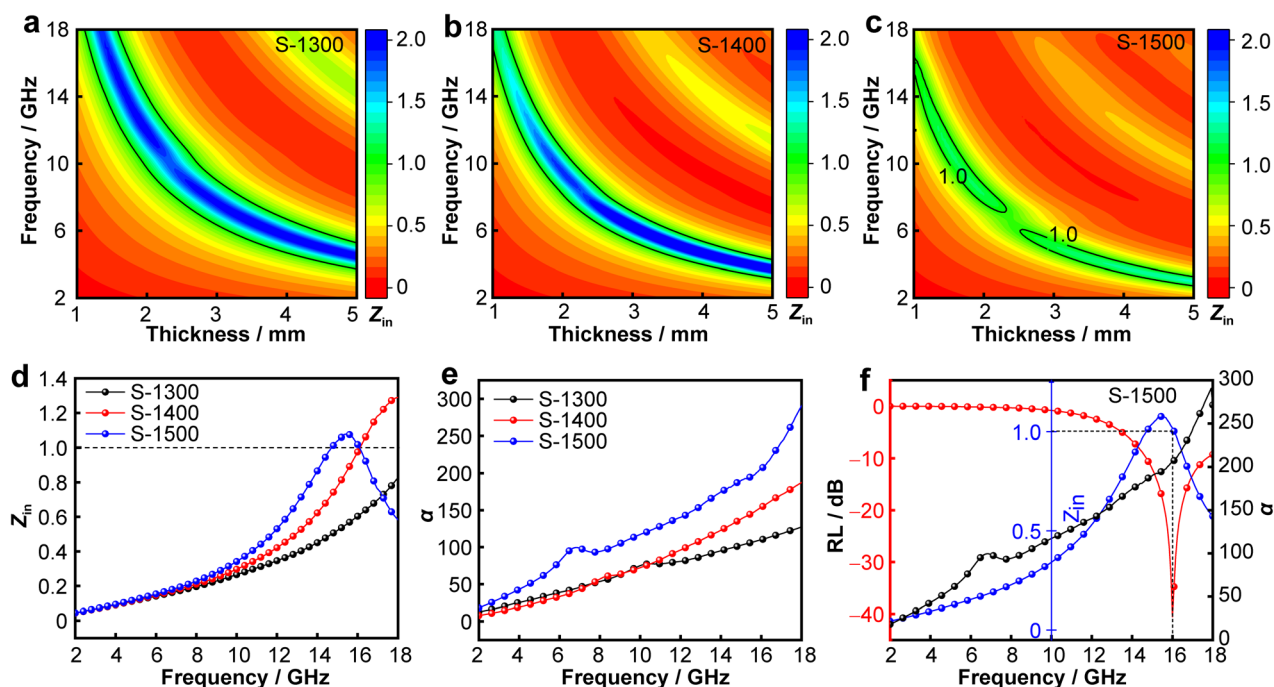
Fig. 7 **a**−**c** 2D impedance matching images; **d** impedance matching curves at thickness of 1.05 mm; **e** attenuation constant curves of Co–SiCN ceramics pyrolyzed at different temperatures; **f** frequency-dependent RL, α, and Z_{in} values for S-1500 sample
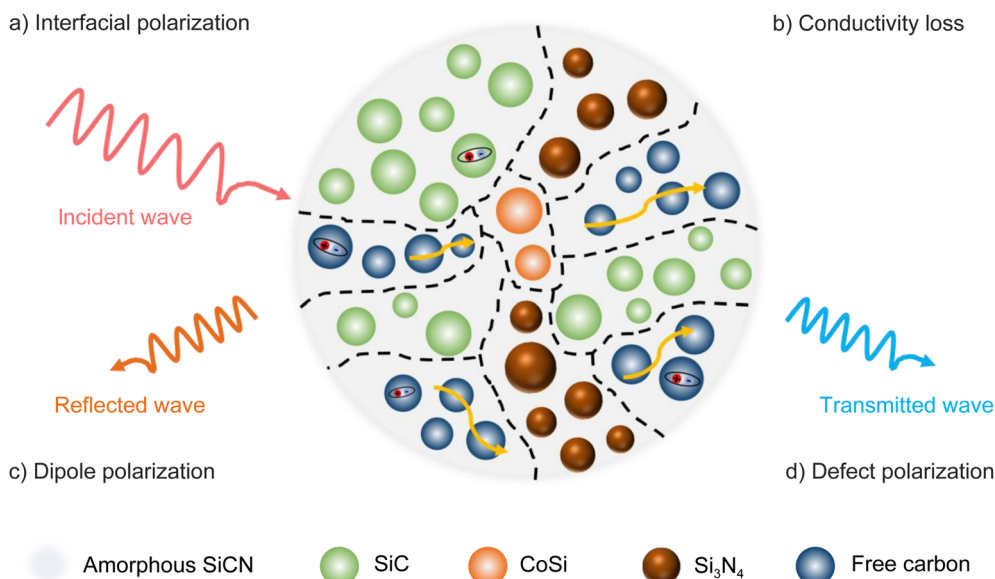
Fig. 8 Proposed microwave absorption mechanism of Co-containing polymer-derived SiCN ceramics

Si_3N_4 phase can be regarded as the A phase, whereas the free carbon, CoSi, and SiC nanocrystals generated in situ in the SiCN matrix with high dielectric properties can be regarded as the B phase. At a pyrolysis temperature of 1500 °C, the carbothermal reaction between free carbon and Si_3N_4 is completely achieved, producing a large amount of SiC. The consumption of Si_3N_4 during this reaction adjusts the permittivity of the ceramic, thereby

enhancing its dielectric loss and EWA ability. First, the dipole polarization of S-1500 includes the intrinsic dipole polarization of SiC and dipole polarization caused by the abundant dangling bonds and lattice defects in the carbon layers. Second, free carbon acts as a high dielectric loss phase with the ability to transform electromagnetic wave energy into heat energy, thereby promoting conductivity loss. Third, the defect polarization of free carbon was

attributed to the existence of lattice defects in the carbon layers. Finally, in addition to the role played by single phases, the coexistence of the high dielectric B phase and low dielectric A phase not only provides good impedance matching but also contributes to the generation of multiple heterogeneous interfaces, which leads to interfacial polarization under certain alternating electromagnetic fields. In other words, the excellent EWA performance of S-1500 can be attributed to the synergistic effect of the low dielectric phase A, which provides electromagnetic waves with easy entry into the ceramic, and the high dielectric phase B, which can attenuate electromagnetic waves via the synergistic effects of dipole polarization, conductivity loss, defect polarization, and interfacial polarization.

4 Conclusion

Co–SiCN ceramics were successfully fabricated by simple physical mixing via a polymer-derived ceramic route. The introduction of ZIF-67 promoted the in situ generation of dielectric loss phases, including SiC and CoSi nanocrystals along with free carbon, which endowed the SiCN ceramics with multiple crystalline phases and optimized their impedance matching and EWA ability. The Co–SiCN ceramic pyrolyzed at 1500 °C exhibited superior EWA performance, with an EAB_{max} of 3.0 GHz at an ultralow thickness of 1.05 mm and RL_{min} of -46.4 dB at a low frequency of 6.0 GHz. The simple preparation method proposed in this study and excellent EWA performance of the obtained ceramics provide new ideas for the development of SiCN-based microwave absorbers.

Declarations

Conflict of interests The authors declare that they have no conflict of interest.

References

[1] Zhao ZH, Zhang LM, Wu HJ. Hydro/organo/ionogels: "controllable" electromagnetic wave absorbers. Adv Mater. 2022; 34(43):2205376. https://doi.org/10.1002/adma.202205376.

[2] Guan XM, Yang ZH, Zhou M, Yang L, Peymanfar R, Aslibeiki B, Ji GB. 2D MXene nanomaterials: synthesis, mechanism, and multifunctional applications in microwave absorption. Small Struct. 2022;3(10):2200102. https://doi.org/10.1002/sstr.202200102.

[3] Chen XT, Zhou M, Zhao Y, Gu WH, Wu Y, Tang SL, Ji GB. Morphology control of eco-friendly chitosan-derived carbon aerogels for efficient microwave absorption at thin thickness and thermal stealth. Green Chem. 2022;24(13):5280. https://doi.org/10.1039/d2gc01604d.

[4] Liang HS, Zhang LM, Wu HJ. Exploration of twin-modified grain boundary engineering in metallic copper predominated electromagnetic wave absorber. Small. 2022;18(38):2203620. https://doi.org/10.1002/smll.202203620.

[5] Hui SC, Zhang LM, Wu HJ. Cationic doping induced sulfur vacancy formation in polyionic sulfide for enhanced electromagnetic wave absorption. J Colloid Interface Sci. 2022. https://doi.org/10.1016/j.jcis.2022.09.078.

[6] Huang XG, Wei JW, Zhang YK, Qian BB, Jia Q, Liu J, Zhao XJ, Feng SG. Ultralight magnetic and dielectric aerogels achieved by metal-organic framework initiated gelation of graphene oxide for enhanced microwave absorption. Nanomicro Lett. 2022; 14(1):107. https://doi.org/10.1007/s40820-022-00851-3.

[7] Chang Q, Liang HS, Shi B, Wu HJ. Microstructure induced dielectric loss in lightweight Fe_3O_4 foam for electromagnetic wave absorption. Science. 2022;25(3):103925. https://doi.org/10.1016/j.isci.2022.103925.

[8] Wang J, Schölch V, Görke O, Schuck G, Wang XF, Shao GF, Schorr SS, Bekheet MF, Gurlo A. Metal-containing ceramic nanocomposites synthesized from metal acetates and polysilazane. Open Ceram. 2020;1:100001. https://doi.org/10.1016/j.oceram.2020.100001.

[9] Sun SJ, Liu YB, Ma Z, Jiao J, Jiao CR, Yang JH. Microstructure and mechanical properties of the ZrB_2–SiC eutectic phase obtained via induction plasma spheroidization. Ceram Int. 2021; 47(20):29120. https://doi.org/10.1016/j.ceramint.2021.07.074.

[10] Zhang YJ, Yin XW, Ye F, Kong L. Effects of multi-walled carbon nanotubes on the crystallization behavior of PDCs-SiBCN and their improved dielectric and EM absorbing properties. J Eur Ceram Soc. 2014;34(5):1053. https://doi.org/10.1016/j.jeurceramsoc.2013.11.044.

[11] Luo CJ, Miao P, Tang YS, Kong J. Excellent electromagnetic wave absorption of MOF/SiBCN nanomaterials at high temperature. Chin J Aeronaut. 2021;34(11):277. https://doi.org/10.1016/j.cja.2020.06.028.

[12] Feng YR, Guo X, Gong HY, Zhang YJ, Liu Y, Lin X, Mao JJ. Microwave absorption performance of PDCs-SiCN(Fe) ceramics with negative imaginary permeability. Ceram Int. 2018; 44(9):10420. https://doi.org/10.1016/j.ceramint.2018.03.058.

[13] Liu Y, Feng YR, Gong HY, Zhang YJ, Lin X, Xie BY, Mao JJ. Microwave absorbing performance of polymer-derived SiCN (Ni) ceramics prepared from different nickel sources. J Alloys Compd. 2018;749:620. https://doi.org/10.1016/j.jallcom.2018.03.346.

[14] Li Q, Yin XW, Duan WY, Cheng LF, Zhang LT. Improved dielectric properties of PDCs-SiCN by in-situ fabricated nano-structured carbons. J Eur Ceram Soc. 2017;37(4):1243. https://doi.org/10.1016/j.jeurceramsoc.2016.11.034.

[15] Li Q, Yin XW, Duan WY, Hao BL, Kong L, Liu XM. Dielectric and microwave absorption properties of polymer derived SiCN ceramics annealed in N_2 atmosphere. J Eur Ceram Soc. 2014; 34(3):589. https://doi.org/10.1016/j.jeurceramsoc.2013.08.042.

[16] Lu JB, Feng YR, Liu J, Liu CM, Tong YC, Wu SG, Sun HB, Gong HY, Guo X. Improved electromagnetic wave absorbing performance of PDCs-SiCN(Ni) fibers with different nickel content. Ceram Int. 2022;48(16):23578. https://doi.org/10.1016/j.ceramint.2022.05.006.

[17] Feng YR, Guo X, Gong HY, Zhang YJ, Lin X. Enhanced electromagnetic microwave absorption of Fe/C/SiCN composite ceramics targeting in integrated structure and function. Ceram

Int. 2021;47(3):3842. https://doi.org/10.1016/j.ceramint.2020.09.244.

[18] Liu MY, Lu JB, Gong HY, Sheng MM, Jing J, Sun S, Wang GT, Miao YL. Enhanced microwave absorbing performance of Ni-containing SiCN ceramics by constructing multiple interfaces and in-situ generating MWCNTs. Ceram Int. 2022;48(22):33871. https://doi.org/10.1016/j.ceramint.2022.07.335.

[19] Xue JM, Ren FY, Dong YP, Wei HJ, Yang F, Cheng LF. Si$_3$N$_4$-BN-SiCN ceramics with unique hetero-interfaces for enhancing microwave absorption properties. Ceram Int. 2021;47(9):12261. https://doi.org/10.1016/j.ceramint.2021.01.075.

[20] Guo X, Xiao FF, Li J, Zhang H, Hu QQ, Li GC, Sun HB. Fe-doped SiCN composite fibers for electromagnetic waves absorption. Ceram Int. 2021;47(1):1184. https://doi.org/10.1016/j.ceramint.2020.08.236.

[21] Jia T, Gu YF, Li FT. Progress and potential of metal-organic frameworks (MOFs) for gas storage and separation: a review. J Environ Chem Eng. 2022;10(5):108300. https://doi.org/10.1016/j.jece.2022.108300.

[22] Zhang ZW, Cai ZH, Wang ZY, Peng YL, Xia L, Ma SP, Yin ZZ, Huang Y. A review on metal-organic framework-derived porous carbon-based novel microwave absorption materials. Nanomicro Lett. 2021;13(1):56. https://doi.org/10.1007/s40820-020-00582-3.

[23] Tao JQ, Xu LL, Jin HS, Gu YS, Zhou JT, Yao ZJ, Tao XW, Chen P, Dinghui W, Li Z, Wu HJ. Selective coding dielectric genes based on proton tailoring to improve microwave absorption of MOFs. Adv Powder Mater. 2023;2(1):100091. https://doi.org/10.1016/j.apmate.2022.100091.

[24] Song CK, Liu YS, Ye F, Wang J, Cheng LF. Microstructure and electromagnetic wave absorption property of reduced graphene oxide-SiC$_{nw}$/SiBCN composite ceramics. Ceram Int. 2020;46(6):7719. https://doi.org/10.1016/j.ceramint.2019.11.275.

[25] Ding CX, Hu DX, He XR, Lai YF, Shao GF. Fabrication and microstructure evolution of monolithic bridged polysilsesquioxane-derived SiC ceramic aerogels. Ceram Int. 2022;48(18):25833. https://doi.org/10.1016/j.ceramint.2022.05.259.

[26] Feng YR, Guo X, Huang K, Elsayed H, Franchin G, Gong HY, Colombo P. Enhanced electromagnetic microwave absorption of SiOC ceramics targeting the integration of structure and function. J Eur Ceram Soc. 2021;41(13):6393. https://doi.org/10.1016/j.jeurceramsoc.2021.06.007.

[27] Shao GF, Shen XD, Huang XG. Multilevel structural design and heterointerface engineering of a host-guest binary aerogel toward multifunctional broadband microwave absorption. ACS Mater Lett. 2022;4(9):1787. https://doi.org/10.1021/acsmaterialslett.2c00634.

[28] Yuan KK, Han DY, Zhao WY, Zhang WW, You GQ, Li ML, Fan BB, Lu HX, Wang HL, Xu HL, Shao G, Zhang R. Structure regulation and microwave absorption property of SiCN ceramic aerogels produced by catalytic pyrolysis. Ceram Int. 2021;47(22):31561. https://doi.org/10.1016/j.ceramint.2021.08.035.

[29] Wang S, Lin X, Ashfaq MZ, Zhang XF, Zhao CC, Sheng MM, Yang RK, Pei YR, Gong HY, Zhang YJ. Microwave absorption properties of SiCN ceramics doped with cobalt nanoparticles. J Mater Sci: Mater Electron. 2020;31(5):3803. https://doi.org/10.1007/s10854-020-02912-y.

[30] Wang S, Gong HY, Zhang YJ, Ashfaq MZ. Microwave absorption properties of polymer-derived SiCN(CNTs) composite ceramics. Ceram Int. 2021;47(1):1294. https://doi.org/10.1016/j.ceramint.2020.08.250.

[31] Liu XM, Yu ZJ, Ishikawa R, Chen LQ, Liu XF, Yin XW, Ikuhara Y, Riedel R. Single-source-precursor derived RGO/CNTs-SiCN ceramic nanocomposite with ultra-high electromagnetic shielding effectiveness. Acta Mater. 2017;130:83. https://doi.org/10.1016/j.actamat.2017.03.031.

[32] Liu XM, Yu ZJ, Ishikawa R, Chen LQ, Yin XW, Ikuhara Y, Riedel R. Single-source-precursor synthesis and electromagnetic properties of novel RGO–SiCN ceramic nanocomposites. J Mater Chem C. 2017;5(31):7950. https://doi.org/10.1039/c7tc00395a.

[33] Li Q, Yin XW, Zhang LT, Cheng LF. Effects of SiC fibers on microwave absorption and electromagnetic interference shielding properties of SiC$_f$/SiCN composites. Ceram Int. 2016;42(16):19237. https://doi.org/10.1016/j.ceramint.2016.09.089.

[34] Huang XG, Qiao M, Lu XC, Li YF, Ma YB, Kang B, Quan B, Ji GB. Evolution of dielectric loss-dominated electromagnetic patterns in magnetic absorbers for enhanced microwave absorption performances. Nano Res. 2021;14(11):4006. https://doi.org/10.1007/s12274-021-3327-x.

[35] Wang P, Liu PA, Ye S. Preparation and microwave absorption properties of Ni(Co/Zn/Cu)Fe$_2$O$_4$/SiC@SiO$_2$ composites. Rare Met. 2016;38(1):59. https://doi.org/10.1007/s12598-016-0752-1.

[36] Qin M, Zhang LM, Wu HJ. Dual-template hydrothermal synthesis of multi-channel porous NiCo$_2$O$_4$ hollow spheres as high-performance electromagnetic wave absorber. Appl Surf Sci. 2020;515:146132. https://doi.org/10.1016/j.apsusc.2020.146132.

[37] Wu Y, Zhao Y, Zhou M, Tan SJ, Peymanfar R, Aslibeiki B, Ji GB. Ultrabroad microwave absorption ability and infrared stealth property of nano-micro CuS@rGO lightweight aerogels. Nanomicro Lett. 2022;14(1):51. https://doi.org/10.1007/s40820-022-00906-5.

[38] Mu ZG, Wei GK, Zhang H, Gao L, Zhao Y, Tang SL, Ji GB. The dielectric behavior and efficient microwave absorption of doped nanoscale LaMnO$_3$ at elevated temperature. Nano Res. 2022;15(8):7731. https://doi.org/10.1007/s12274-022-4500-6.

[39] Huang XG, Yu GY, Zhang YK, Zhang MJ, Shao GF. Design of cellular structure of graphene aerogels for electromagnetic wave absorption. Chem Eng J. 2021;426:131894. https://doi.org/10.1016/j.cej.2021.131894.

[40] Pan HX, Yin XW, Xue JM, Cheng LF, Zhang LT. In-situ synthesis of hierarchically porous and polycrystalline carbon nanowires with excellent microwave absorption performance. Carbon. 2016;107:36. https://doi.org/10.1016/j.carbon.2016.05.045.

[41] An J, Zhao CY, He ZJ, Mu X, Guo SH, Xu LH, He J, Zhao DL. Synthesis and microwave absorption property of nanostructured Ketjen black/Fe$_3$O$_4$ core/shell particles. Rare Met. 2022;41(10):3351. https://doi.org/10.1007/s12598-022-02046-6.

[42] Wu XM, Xie F, Yao YL, Sun Y, Hua ZS, Zhao Z, Yang YX. Template-free preparation of porous Co microfibers from spent lithium-ion batteries as a promising microwave absorber. Rare Met. 2022;41(10):3475. https://doi.org/10.1007/s12598-022-02034-w.